Published in "Macromolecules 41(22): 8759–8769, 2009"
which should be cited to refer to this work.

Poly[2,7-(9,9-dihexylfluorene)]-*block*-poly(2-vinylpyridine) Rod−Coil and Coil−Rod−Coil Block Copolymers: Synthesis, Morphology and Photophysical Properties in Methanol/THF Mixed Solvents

Chia-Hung Lin,[†] Yi-Chih Tung,[†] Janne Ruokolainen,[‡] Raffaele Mezzenga,*[,§,⊥,∥] and Wen-Chang Chen*[,†,⊥]

Department of Chemical Engineering, National Taiwan University, Taipei, Taiwan, Department of Engineering Physics, Helsinki University of Technology, P.O. Box 5100, 02015 TKK, Finland, Department of Physics and Fribourg Center for Nanomaterials, University of Fribourg, Perolles, Fribourg, CH-1700 (Switzerland), Nestlé Research Center, Vers-Chez-les-Blanc, 1000 Lausanne 26, Switzerland, and Institute of Polymer Science and Engineering, National Taiwan University, Taipei, Taiwan

ABSTRACT: New rod−coil diblock and coil−rod−coil triblock copolymers containing conjugated poly[2,7-(9,9-dihexylfluorene)] (PF) and coil-like poly(2-vinylpyridine) (P2VP) were synthesized by combining coupling reaction and living anionic polymerization. Scanning force microscopy (SFM), transmission electron microscopy (TEM), cryo-transmission electron microscopy (cryoTEM), and dynamic light scattering (DLS) were used to obtain the morphologies of the aggregates in selective solvents of different methanol(MeOH)/tetrahydrofuran (THF) compositions. The effects of micellar morphologies on the photophysical properties were studied by optical absorption and photoluminescence (PL). The experimental results showed that the diblock PF-*b*-P2VP (**di-PFPVP**) maintained spherical micellar aggregates as the MeOH content increased. However, the triblock PF-*b*-P2VP(**tri-PFPVP**) were found to readily aggregate in elongated cylinders due to its symmetric structure. Consequently, **tri-PFPVP** polymer chains could stack together favorably and have stronger $\pi-\pi$ interchain stacking compared with **di-PFPVP**, leading to the higher absorption wavelength maximum. The quantum efficiencies were gradually quenched with increasing the MeOH content for both copolymers. Moreover, for **di-PFPVP**, the increase of the MeOH content induced a blue shift in both absorption and PL spectra, suggesting an "H-type" aggregation. However, **tri-PFPVP** exhibited a blue shift in absorption but a red shift in PL by increasing the MeOH content, which reflected a different type of aggregation. The present study revealed the effects of polymer chain architecture and the aggregated structures of the rod−coil block copolymers on the photophysical properties.

Introduction

Amphiphilic block copolymers have stimulated extensive research interest in recent years since they can self-assemble to form ordered nanostructures in bulk, thin films or solutions.[1−18] Such block copolymer assemblies have potential applications in thermoplastic elastomers, pressure-sensitive adhesives, colloidal dispersants, drug delivery, separation membranes, etc. An interesting subject in amphiphilic block copolymers is the formation of multiple morphologies in dilute solution.[1−10] The driving forces governing the morphological transformation include the relative block length, block polarity, volume fraction, chain flexibility, temperature, initial polymer concentration, mixed solvent composition, additives, etc.

Amphiphilic conjugated rod−coil block copolymers have attracted great attention for optoelectronic or sensory applications due to their unusual morphologies and photophysical properties in both solution and solid state.[19−34] The high immiscibility and stiffness asymmetry between the rigid rod and flexible coil segments profoundly affect the molecular packing in thermodynamically stable states and lead to the formation of self-organized structures.[19−21] Aggregation and microphase separation of conjugated rod−coil block copolymers could yield a number of nanoscale morphologies, such as lamellar, spherical, cylindrical, and vesicular structures with tunable optical and electronic properties in dilute solution. Also, solvatochromatic behaviors were exhibited through aggregation-induced $\pi-\pi$ stacking and planarization of the conjugated segments.[22]

Different conjugated moieties of π-conjugated rod−coil block copolymers were reported in the literature, including thiophene, phenylene, quinoline, fluorene, etc.[23−28] Polyfluorene is one of the widely studied conjugated polymers for optoelectronic applications due to high fluorescence quantum yields, good thermal and chemical stability in both solution and solid state.[29,30] Several examples of polyfluorene-based rod−coil block copolymers were prepared by atom transfer radical polymerization (ATRP),[31−35] such as polyfluorene-*block*-poly(methacrylic acid) (PF-*b*-PMAA), PF-*block*-poly(2-(dimethylamino)ethyl methacrylate) (PF-*b*-PDMAEMA), PF-*block*- poly(2-(9-carbozolyl)ethyl methacrylate (PF-*b*-PCzEMA), and PF-b-Poly(2-hydroxyethyl methacrylate) (PF-*b*-PHEMA). We observed multiple morphologies from poly[2,7-(9,9-dihexylfluorene)]-*block*-poly(acrylic acid) (PF-*b*-PAA) in dilute solutions of dichloromethane/methanol by varying the PAA coil length or methanol content, including large compound micelle (LCMs), sphere, or vesicles.[36] Such morphological transformations could induce a significant variation of optical absorption or fluorescence characteristics because of possible H-aggregation formation. However, only limited examples of polyfluorene based rod−coil block copolymers have been synthesized by living anionic polymerization owing to the difficult synthetic procedure

* To whom all correspondence should be addressed. E-mail: (R.M.) raffaele.mezzenga@unifr.ch; (W.-C.C.) chenwc@ntu.edu.tw.
[†] Department of Chemical Engineering, National Taiwan University.
[‡] Department of Engineering Physics, Helsinki University of Technology.
[§] Department of Physics and Fribourg Center for Nanomaterials, University of Fribourg.
[∥] Nestlé Research Center.
[⊥] Institute of Polymer Science and Engineering, National Taiwan University.

Scheme 1. Synthetic Routes of the Rod−Coil Diblock PF-*b*-P2VP

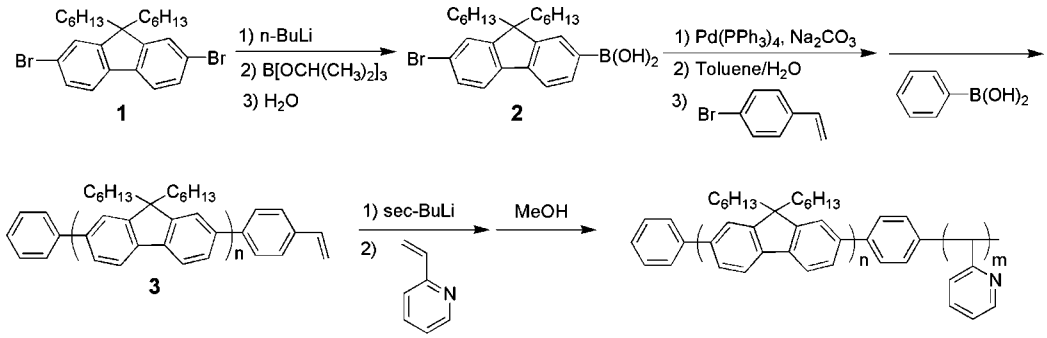

Scheme 2. Synthetic Routes of the Coil−Rod−Coil Triblock P2VP-*b*-PF-*b*-P2VP

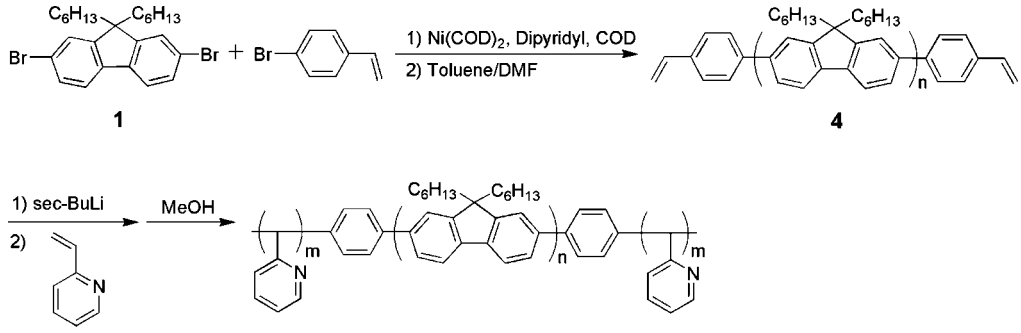

involved,[37] although living anionic polymerization were widely used to prepare well-defined block copolymers.[38−40]

In this study, new rod−coil diblock and coil−rod−coil triblock copolymers were synthesized by combining coupling reaction for the poly[2,7-(9,9-dihexylfluorene)] (PF) rod and living anionic polymerization for the very weak acceptor poly(2-vinylpyridine) (P2VP) coil, as shown in schemes 1 and 2. Self-assembly in bulk of rod−coil block copolymers with poly-(diethylhexyloxy-p-phenylene vinylene) as a rod and poly(4-vinylpyridine) as a coil PPV-P4VP, was studied in our previous work.[41] However, to the best of our knowledge, the present study is the first report on synthesis and self-assembly in selective solvents of diblock and triblock copolymers based on poly[2,7-(9,9-dihexylfluorene)] and poly(2-vinylpyridine). By changing the selectivity of the solvent via varying THF/methanol ratios, diverse aggregated morphologies and different optical characteristics in solution were induced. In an attempt to correlate the morphologies of the aggregates with their optical properties, we have combined structural and photophysical techniques such as room temperature and cryo-transmission electron microscopy (TEM, cryoTEM), scanning force microscopy (SFM), dynamic light scattering (DLS), UV−vis optical absorption and photoluminescence (PL).

Experimental Section

Materials. 9,9-dihexyl-2,7-dibromofluorene (**1**) (97%, Aldrich), triisopropyl borate (>98%, Aldrich), tetrakis(triphenylphosphine)-palladium(0) ($Pd(PPh_3)_4$)) (Aldrich), sodium carbonate (Na_2CO_3) (Aldrich), 4-bromostyrene (98%, Aldrich), phenylboronic acid (97%, Aldrich), bis(1,5-cyclooctadiene)nickel(0) ($Ni(COD)_2$) (Aldrich), 1,5-cyclooctadiene (COD) (99%+, Aldrich), 2,2′-dipyridyl (Aldrich), and *n*- and *sec*-butyllithium (1.3 M in cyclohexane/hexane (92/8), Acors) were used without further purification. Toluene (anhydrous), *N*,*N*-dimethylformamide (DMF) (anhydrous), and methanol (MeOH) were purchased from TEDIA and used as received. 2-vinylpyridine (2VP, Acros, purity 97%) was distillated from CaH_2 powder and dibutylmagnesium (Aldrich, 1.0 M solution in heptane) under reduced pressure. Tetrahydrofuran (THF, Acros, 99.9%) was distillated from sodium (Aldrich, 30−35 wt % dispersion in paraffin wax) and benzophenone (Aldrich, 99+%) mixture. Poly(2-vinyl pyridine) (P2VP) used for comparison was synthesized by conventional protocol using living anionic polymerization (M_n = 13000, PDI = 1.08).

Synthesis of Rod−Coil Diblock PF-*b*-P2VP Copolymers. The synthetic route of diblock PF-*b*-P2VP is shown in Scheme 1 and described below:

*9,9-Dihexyl-2-phenyl-7-(4-vinylphenyl)-9H-fluorene (**3**).* 2-bromo-9,9-di-n-hexylfluoreneboronic acid (**2**) was prepared by monolithiation of 9,9-dihexyl-2,7-dibromofluorene (**1**) with 1.1 equiv of *n*-butyllithium followed by boronation with triisopropyl borate at −78 °C, according to the literatures.[36] 9,9-Dihexyl-2-phenyl- 7-(4-vinylphenyl)-9*H*-fluorene (**3**) was synthesized by modified Suzuki coupling protocol.[37] A 3.0 g (6.55 mmol) sample of compound **2**, 56 μL (0.542 mmol) of 4-bromostyrene, 80 mg (0.070 mmol) of tetrakis(triphenylphosphine)palladium(0) and 5 drops of Aliquat 336 were reacted in toluene and 2 M Na_2CO_3 mixtures under reflux at 80 °C. After heating and stirring vigorously for 24 h, 1.5 equiv of phenylboronic acid were added as end-capping reagent for bromoside. The resulting polymers were precipitated into 500 mL of MeOH, filtered, and dried under vacuum at 45 °C for 36 h. (Yields: 75%.) ^{1}H NMR ($CDCl_3$), δ (ppm): 7.3−7.9 (10H, ring aromatic protons and phenyl end group), 2.1 (2H, $-\underline{CH_2}C_5H_{11}$), 1.1 (8H, $-CH_2(\underline{CH_2})_4-CH_3$), 0.7 (3H, $-(CH_2)_5\underline{CH_3}$), 5.3, 5.8, 6.8 (vinyl protons of end-caps). Gel permeation chromatography (GPC): M_n = 5130, PDI = 1.83.

Poly[2,7-(9,9-dihexylfluorene)]-block-poly(2-vinylpyridine) (PF-b-P2VP, di-PFPVP). Amphiphilic diblock copolymer of PF-*b*-P2VP was synthesized by living anionic polymerization, similar to that reported in the literature.[25] 150 mg (∼0.04 mmol) of PF macro-initiator (**3**) was dried in a reaction flask under high vacuum environment (∼10^{-3} Torr) to remove the residual solvent for 2 h. Distilled THF via *sec*-BuLi as purifying agent was transferred to the reaction flask. Excess *sec*-BuLi was then used as initiator and added into the reaction mixtures at −78 °C using a syringe. A deep black color is an indication that the vinyl-end capping PF was initiated completely. In order to quench the effect of the residual *sec*-BuLi, the reaction was allowed to warm up to the room temperature for 0.5 h. At the same time, the excess *sec*-BuLi reacted with THF to form ethylene and lithium salt. Then, purified 2VP

monomer was added into the reaction flask rapidly at −78 °C and polymerized for 1 h. Finally, the polymerization reaction was terminated by adding a small amount of MeOH and precipitated in hexane. The yellow-green polymer powder was collected and then dried under vacuum at 45 °C to remove the residual solvent. (Yields: 95%.) ^{1}H NMR ($CDCl_3$), δ (ppm): 7.4−7.9 (10H, ring aromatic protons and phenyl end group), 6.0−7.5, 8.0−9.0 (4H, pyridine ring aromatic protons), 1.5−2.5 (5H, $-\underline{CH_2}C_5H_{11}$, $-\underline{CH_2}CHC_5H_4N$), 1.1 (8H, $-CH_2(\underline{CH_2})_4-CH_3$), 0.7 (3H, $-(CH_2)_5\underline{CH_3}$). GPC: M_n = 21290, PDI = 1.33.

Synthesis of Coil−Rod−Coil Triblock P2VP-*b*-PF-*b*-P2VP Copolymers. The synthetic route of triblock P2VP-*b*-PF-*b*-P2VP is shown in Scheme 2 and described below.

*9,9-dihexyl-2,7-bis(4-vinylphenyl)-9H-fluorene (***4***).* Divinyl end-capped-polyfluorene (**4**) was prepared according to the literature report using modified Yamamoto coupling methods.[42] 970 mg (3.5 mmol) of $Ni(COD)_2$, 0.45 mL (3.5 mmol) of COD, and 598 mg (3.5 mmol) of 2,2′-dipyridyl (molar ratio = 1:1:1) were dissolved in 12 mL of DMF and 12 mL of toluene mixtures and heated under N_2 at 80 °C for 0.5 h. 9,9-Dihexyl-2,7-dibromofluorene (**1**) (861 mg, 1.75 mmol) and 4-bromostyrene as end-capper (57 μL, 0.44 mmol) were mixed in 10 mL of degassed toluene and then added into the above solution, and the polymerization was maintained at 80 °C for 24 h. After the polymerization, the polymers were precipitated in an equivalent volume of a mixture constituted of concentrated HCL, MeOH and acetone. The isolated polymers were then dissolved in chloroform and reprecipitated in MeOH. The filtered polymer powder was dried at 60 °C under vacuum. (Yields: 80%.) ^{1}H NMR ($CDCl_3$), δ (ppm): 7.3−7.9 (10H, ring aromatic protons and phenyl end group), 2.1 (2H, $-\underline{CH_2}C_5H_{11}$), 1.1 (8H, $-CH_2(\underline{CH_2})_4-CH_3$), 0.7 (3H, $-(CH_2)_5\underline{CH_3}$), 5.3, 5.8, 6.8 (vinyl protons of end-caps). GPC: M_n = 4620, PDI = 1.88.

Poly(2-vinylpyridine)-block-poly[2,7-(9,9-dihexylfluorene)]-block-poly(2-vinylpyridine) (P2VP-b-PF-b-P2VP, tri-PFPVP). A 200 mg (∼0.06 mmol) sample of PF macroinitiator (**4**) was dried in the reaction flask under high vacuum environment (∼10^{-3} Torr) to remove the residual solvent for 2 h. Purified THF was transferred to the reaction flask and then excess *sec*-BuLi was added into the reaction mixtures at −78 °C by using a syringe. A deep black color is an indication that the PF vinyl-end was initiated completely. The reaction mixtures were allowed to warm up to the room temperature for 0.5 h. Then, purified 2VP monomer, was added into the reaction flask rapidly at −78 °C and polymerized for 1 h. Finally, the polymerization reaction was terminated by adding a small amount of MeOH and precipitated in hexane. The yellow-green polymer powder was collected and then dried via vacuum at 60 °C to remove the residual solvent. (Yields: 95%). ^{1}H NMR ($CDCl_3$), δ (ppm): 7.4−7.9 (10H, ring aromatic protons and phenyl end group), 6.0−7.5, 8.0−9.0 (4H, pyridine ring aromatic protons), 1.5−2.5 (5H, $-\underline{CH_2}C_5H_{11}$, $-\underline{CH_2}CHC_5H_4N$), 1.1 (8H, $-CH_2(\underline{CH_2})_4-CH_3$), 0.7 (3H, $-(CH_2)_5\underline{CH_3}$). GPC: M_n = 16530, PDI = 1.56.

Preparation of Block Copolymer Aggregates in Dilute Solutions. Sample solutions were prepared by first dissolving the copolymers in the good solvent for both blocks, THF, with an initial polymer concentration of 0.8 mg/mL. The solutions were kept stirring overnight to make them homogeneous. Then, a given weight of MeOH, a selective solvent for P2VP, was added dropwise into the copolymer/THF mixtures under moderate mechanical stirring. The micellar solutions were prepared from the solvent mixture of MeOH/THF with different weight composition from 0/100, 10/90, 30/70, 50/50, 70/30, 90/10 or others. The final polymer concentration was maintained at 0.05 mg/mL and kept stirring for 3 days to reach equilibrium morphologies before characterization.

Characterization. ^{1}H NMR spectra were recorded at room temperature on a Bruker AM 500 (500 MHz) spectrometer using the residual proton resonance of the deuterated chloroform as the internal standard. Molecular weight distribution was determined by gel permeation chromatography (GPC) using a Laboratory Alliance RI2000 instrument (MIXED-D from Polymer Laboratories) connected with one refractive index detector from Schambeck SFD Gmbh. All GPC analyses were performed on polymer/THF solution at a flow rate of 1 mL/min at 40 °C and calibrated with polystyrene. Thermal analyses were carried out on a differential scanning calorimetry (DSC) from TA instrument (TA Q100) with heating cycle from −10 to +200 °C at the heating rate of 20 °C/min and a thermal gravimetric analyzer (TGA) from Perkin-Elmer 7 with heating range from 70 to 800 °C at a heating rate of 20 °C/min.

The aggregated morphologies were visualized both on samples cast from dilute solutions by transmission electron microscopy (TEM) and scanning force microscopy (SFM), and on vitrified solutions by cryoTEM. Standard TEM was performed using a JEOL 1230 operated at an acceleration voltage of 100 kV. A drop of the dilute solution was put on the carbon grid deposited and subsequently blotted with filter paper to remove the excess solution. All the samples were dried under vacuum before characterization. While the first two methods allowed to image the micelles having gone through an evaporation process, cryoTEM allowed real-space imaging of the micelles in their solvated conditions. For cryo-TEM study on micelles dispersions in presence of THF/MeOH solvent, 400 mesh copper grids with a few drops of polymer solution at a concentration of 10 mg/mL were transferred to an environmental chamber FEI vitrobot, and vitrified in a mixture of liquid ethane/propane (−180 °C). Vitrified samples were cryo-transferred into FEI Tecnai 12 transmission electron microscope using Gatan 910 cryo-transfer holder, whose temperature was maintained at −185 °C. Samples were imaged by TEM operated at an acceleration voltage of 120 kV using bright field mode. Micrographs were recorded using Gatan UltraScan 1000 camera having CCD size of 2048 × 2048 pixels.

The surface morphologies of the micelles after solvent evaporation were characterized by a tapping mode scanning force microscopy (TM-SFM) (Nanoscope 3D, Digital instruments Multimode SPM system, USA). The cantilever used was fabricated from phosphorus doped silicon with a spring constant of 3 N/m and a resonance frequency of 83 kHz. For sample preparation, a few drops of the dilute solution were spin-coated (1000 rpm, 30 s) onto the freshly cleaved wafer substrates and then dried in air and at room temperature for 2 h before characterization. The experiments were performed in air and at room temperature.

Dynamic light scattering of micellar solutions was carried out on a beam-line with a ALV-5000 fast correlator in combination with a monomode fiber compact goniometer system and an argon-ion Laser Coherent Innova 308 (λ = 532 nm). Correlation functions were acquired at an angle of 50° and concentrations of 10 mg/mL. The exponential fit used to extract the hydrodynamic radius was performed assuming the viscosity of all solution mixtures to be identical to that of THF.

UV−vis absorption and photoluminescence (PL) spectra were recorded with UV−vis−NIR spectrophotometer (Jasco, V-570) and Fluorolog-3 spectrofluorometer (Jobin Yvon), respectively. The PL efficiency of the solution micelles was recoded by using the diluted quinoline solution in 0.1 N H_2SO_4 as the standard, assuming that the fluorescence quantum efficiency was 0.546 with the excitation wavelength of 370 nm.

Results and Discussion

Polymer Structure Characterization. The chemical structures of the polymers synthesized were confirmed by ^{1}H NMR and GPC. Figure 1(A) shows proton signals of the macroinitiator of diblock PF-*b*-P2VP (**di-PFPVP**), 9,9-dihexyl-2-phenyl-7-(4-vinylphenyl)-9*H*-fluorene (**3,** in Scheme 1) in *d*-chloroform. The proton peaks of the aromatic ring and alkyl group on the PF moiety are shown at 7.3−8.0 and 0.5−2.3 ppm, respectively. The proton signals on the vinyl moiety of macroinitiator **3** are clearly observed in the regions of 5.3, 5.8, and 6.8 ppm, implying the successful incorporation of the end-capper 4-bromostyrene. The proton peaks of vinyl moieties at 5.3 and 5.8 ppm are completely disappeared in the ^{1}H NMR spectrum of **di-PFPVP**, as showed Figure 1B. In addition, proton signals on the pyridine ring of the P2VP moiety are observed at 6.0−7.5 and 8.0−9.0 ppm, respectively. The results clearly suggest the

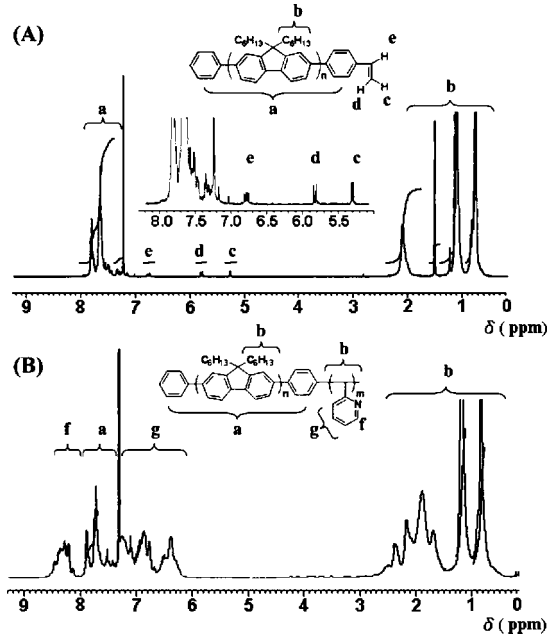

Figure 1. ^{1}H NMR spectra of (A) monoend-functionalized PF-vinyl macroinitiator (**3**) and (B) **di-PFPVP** in $CDCl_3$.

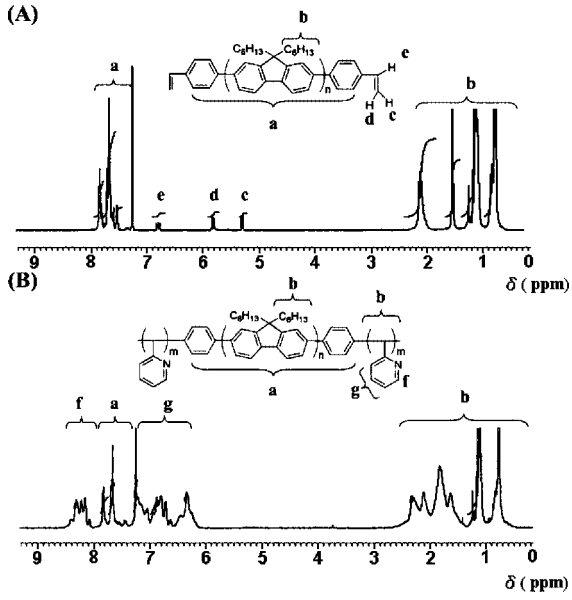

Figure 2. ^{1}H NMR spectra of (A) diend-functionalized PF-vinyl macroinitiator (**4**) and (B) **tri-PFPVP** in $CDCl_3$.

successful preparation of diblock PF-*b*-P2VP (**di-PFPVP**). The ^{1}H NMR spectra of the macroinitiator (9,9-dihexyl-2,7-bis(4-vinylphenyl)-9*H*-fluorene **(4)** and triblock copolymer, **tri-PFPVP**, are shown in Figure 2. Vinyl protons at the two chain ends of PF moiety of the **tri-PFPVP** (Figure 2A) are observed at the similar position as those of **di-PFPVP** but with stronger signal intensities due to its double end-cappers on the PF. The disappearance of the vinyl protons and the observation of pyridine ring protons at 6.0−7.5 and 8.0−9.0 ppm in Figure 2B suggest the successful preparation of **tri-PFPVP**.

In Figure 3, profile a represents the GPC curve of PF macroinitiator (**3,** in Scheme 1). The GPC curve of the first addition of the 2VP monomer shifts to a lower retention time (profile b) and move further by adding more 2VP (profile c), implying the successful polymerization of the 2VP monomer into the PF macroinitiator. The number average molecular weight (M_n) and polydispersity (PDI) of **di-PFPVP** estimated

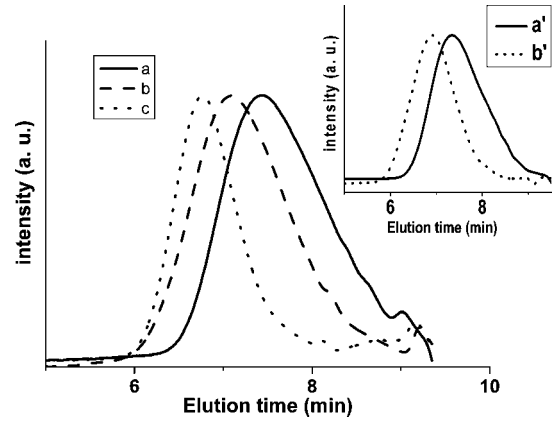

Figure 3. GPC profiles of the synthesized polymers:. (a) monoend-functionalized PF-vinyl macroinitiator, (b) di-PF-*b*-P2VP (first addition of 2VP), (c) di-PF-*b*-P2VP (second addition of 2VP). The inset figure shows the GPC profile of the synthesized polymers: (a′) diend-functionalized PF-vinyl macroinitiator), and (b′) tri-P2VP-*b*-PF-*b*-P2VP.

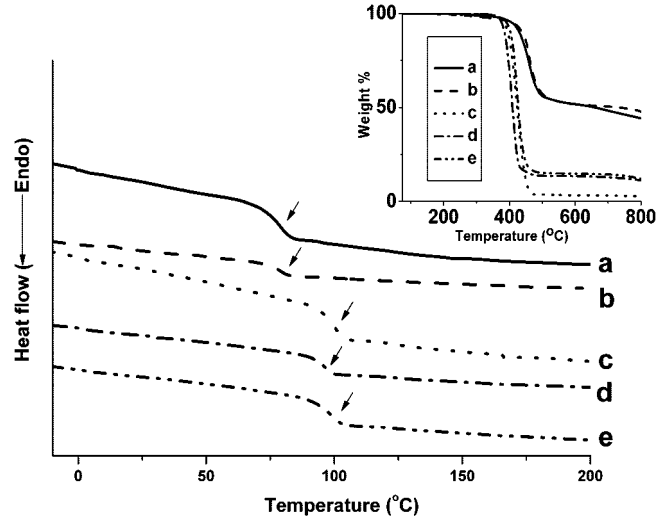

Figure 4. DSC thermograms of (a) PF-vinyl macroinitiator (**3**), (b) PF-vinyl macroinitiator (**4**), (c) pure P2VP, (d) di-PF-*b*-P2VP, and (e) tri-P2VP-*b*-PF-*b*-P2VP. The inset shows the TGA curves of the above corresponding five polymers.

from GPC are 21290 and 1.33, respectively. The estimated molar ratio of the PF block is 0.24. The inset of Figure 3 shows GPC profiles of the **tri-PFPVP**, which shows a similar shifting with the addition of the 2VP monomer. The M_n and PDI of **tri-PFPVP** estimated from GPC are 16530 and 1.33, respectively. The molar ratio of PF segments in the **tri-PFPVP** is estimated to be 0.28, which is similar to **di-PFPVP**. The studied two copolymers with a similar composition were used to study the architecture effect on solution morphology and photophysical properties.

Thermal properties of polymers were examined by TGA and DSC and shown in the Figure 4. In the inset of Figure 4, the thermal degradation temperatures (T_d) (weight loss of 5%) of (a) PF-vinyl macroinitiator (diblock, **3**), (b) PF-vinyl macroinitiator (triblock, **4**), (c) P2VP homopolymer, (d) **di-PFPVP**, and (e) **tri-PFPVP** are observed at 408, 410, 383, 376, and 392 °C, respectively. The glass transition temperatures (T_g) of the above five polymers from the DSC curves are found at 79, 80, 97, 97, and 97 °C, respectively. The T_d and T_g of the two block copolymers are close to the P2VP homopolymer since the molecular weight of the P2VP moiety is much larger than that of the PF moiety.

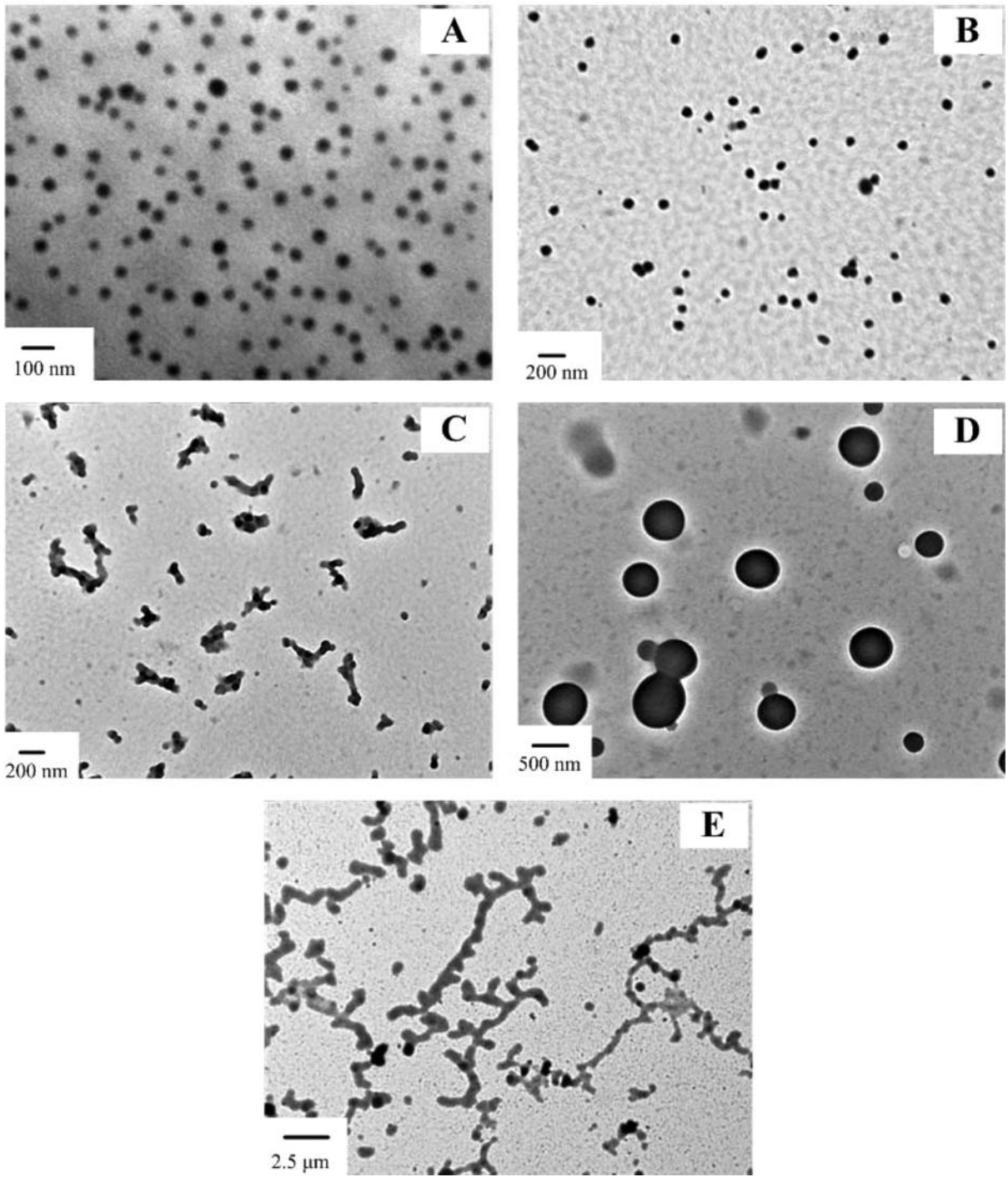

Figure 5. TEM images on morphological changes of **di-PFPVP** in dilute solution by varying MeOH/THF weight compositions (w/w): (A) 10/90, (B) 30/70, (C) 50/50, (D) 70/30, and (E) 90/10.

Micellar Morphologies in Dilute Solution. A structural characterization on the PF-*b*-P2VP copolymers in selective solvents was carried out by studying their micellar aggregation behavior. Figure 5 shows the TEM images on the micellar morphologies of **di-PFPVP** in the solvent mixture of MeOH/THF with different weight composition of 10/90, 30/70, 50/50, 70/30, and 90/10, respectively. Spherical micelles with the diameter around 50 nm are observed at the MeOH concentration of 10 wt % (Figure 5A). By increasing the MeOH content to 30 wt %, significant morphological transformation is not observed but the sizes of spherical micelles grow to nearly 100 nm (Figure 5B). By further increasing the MeOH content, the morphology changes from the aggregation of the spherical micelles (50 wt % MeOH, Figure 5C); the large compound micelles (LCMs) with the diameter near 500 nm (70 wt % MeOH, Figure 5D); to the worm-like structures (90 wt % MeOH content Figure 5E) at the highest MeOH content.

A rationalization of the morphological transformation shown in Figure 5 induced by varying the MeOH content can be realized based on previous findings for the systems of rod−coil PF-b-PAA and coil-coil PS-b-PAA in dilute solution.[36,43−45] The solvent quality becomes progressively poor for the conjugated PF core block by increasing the MeOH content, which leads to enhanced interfacial tension and interfacial energy. In response to such energy increase, the system tends to decrease the total interfacial area by increasing the micellar radius. Thus, the aggregated dimensions of spheres are expected to increase, while the selective solvent (methanol in this study) is added.

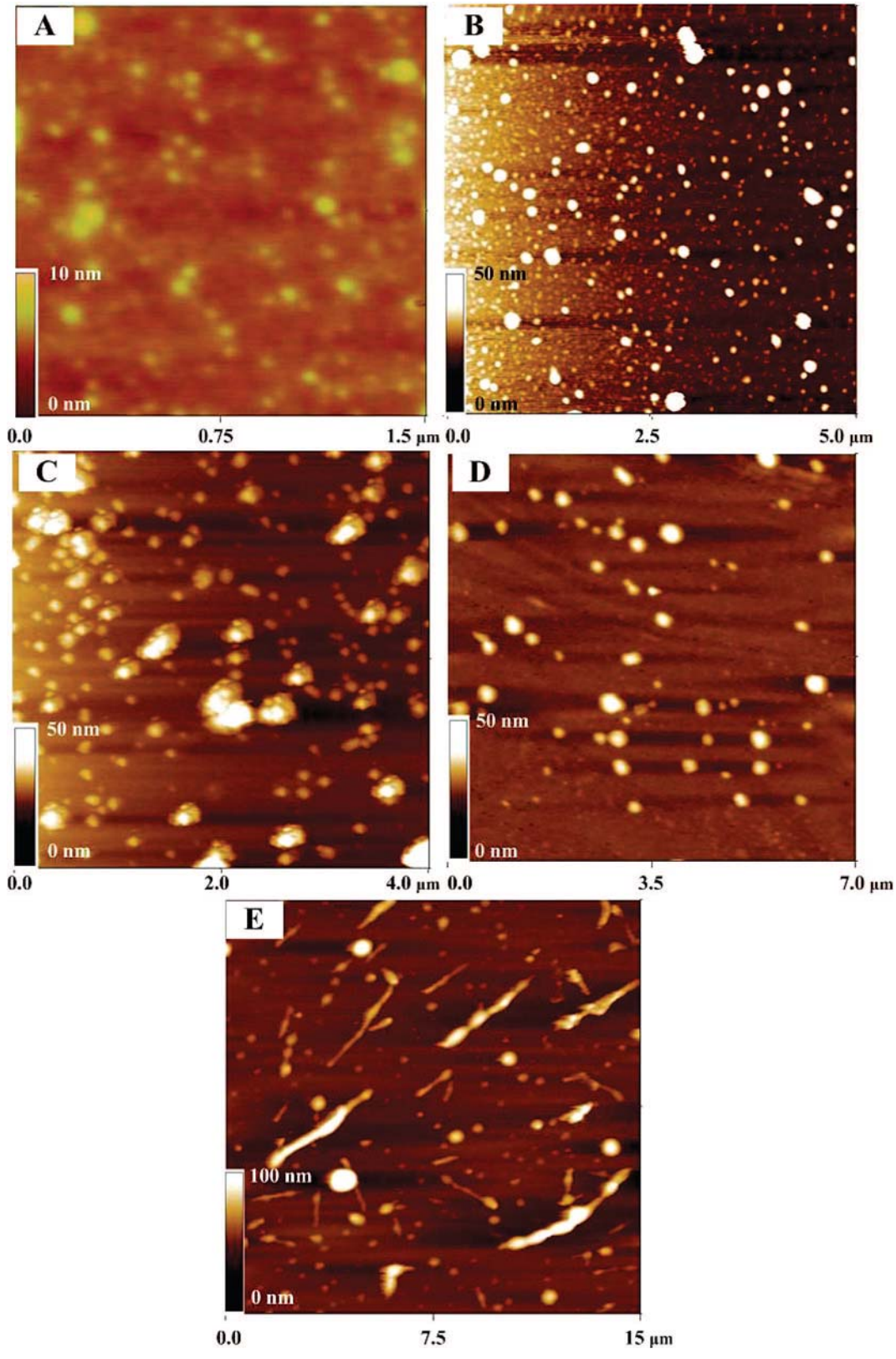

Figure 6. TM-SFM height images on the micellar morphologies of **di-PFPVP** in dilute solution by varying MeOH/THF compositions(w/w): (A) 10/90, (B) 30/70, (C)50/50, (D) 70/30, and (E)90/10.

Thus, a lower number of micelles is observed in Figure 5(D) compared to Figure 5(A), (B) and (C) due to the enhanced aggregation number of polymer chains in each individual micelle. The large compound micelle shown in Figure 5(D) is probably due to the secondary aggregation of spherical micelles. The worm-like morphology in Figure 5(E) is presumably arising from a coalescence of spherical micelles.

Figure 6 shows the tapping mode TM-SFM height images of **di-PFPVP** prepared from the same MeOH content in the solvent mixture of MeOH/THF with different weight composition of 10/90 (Figure 6A), 30/70 (6B), 50/50 (6C), 70/30 (6D), and 90/10 (6E), respectively. Spherical morphologies with the estimated diameter of 50 nm are observed in Figure 6A. The TM-SFM images of Figure 6B−D show spheres, aggregated

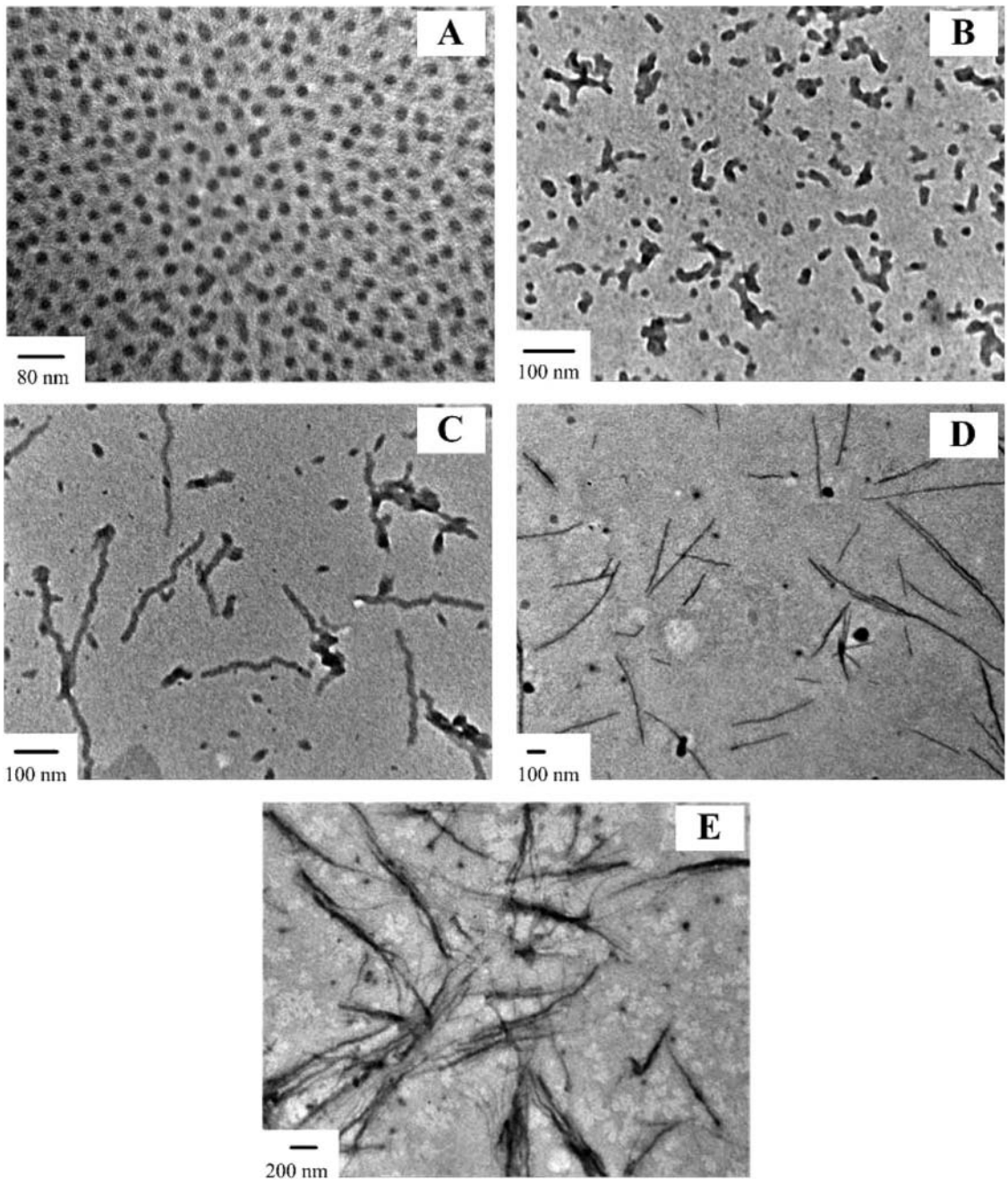

Figure 7. TEM images on morphological changes of **tri-PFPVP** in dilute solution by varying MeOH/THF compositions (w/w): (A) 10/90, (B) 30/70, (C) 50/50, (D) 70/30, and (E) 90/10.

spheres and LCMs morphologies, which are in a good agreement with TEM results. Moreover, the worm-like structures are also captured in the TM-SFM micrograph in Figure 6E. The above results indicate the good stability of micellar structures, not only deposited on the on the copper grids but also onto the surface of wafer used as substrate for SFM studies.[46,47]

Aggregated structures of tri-P2VP-*b*-PF-*b*-P2VP (**tri-PFPVP**) in the THF/MeOH mixed solvent were also examined by TEM and TM-SFM instruments. Figure 7 shows the TEM images of **tri-PFPVP** in different compositions of the MeOH/THF mixtures. Discrete spherical micelles with the estimated diameter of 35 nm and aggregated spheres are shown in Figure 7(A) and (B), respectively at MeOH/THF ratios of 10/90 and 30/70. However, at 50/50 MeOH/THF composition (Figure 7(C)), micelles with an irregular cylindrical shape and with a diameter estimated at 30 nm are observed, as opposed to the diblock micelles observed in the homologue solutions. By further increasing the MeOH/THF ratio to 70/30, micelles with a regular cylindrical shape with $\sim\mu$m scaled contour length are shown in Figure 7(D). Bundles of cylinders are observed in the MeOH/THF ratio of 90/10 as a result of the aggregation of cylindrical micelles (Figure 7(E)).

As discussed above, the system tends to decrease the total interfacial area by increasing the micellar radius with increasing selective solvent content. However, core size also increases leading to a flattening of the interface with subsequent polymer chain stretching and conformational entropy loss, resulting in an increase of total free energy. The change in shape from spherical to cylindrical is an efficient way to minimize total surface area and relax chain stretching. Furthermore, in the case of **tri-PFPVP**, molecular packing into long cylindrical micelles rather than spherical micelles of large size would impose severe topological constrictions, as both external blocks of P2VP have to be exposed to the solvent. Figure 8 sketches the mechanisms

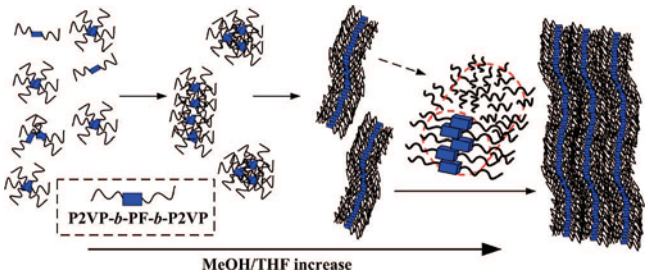

Figure 8. Scheme on the formation of long cylindrical and bundle of cylinders structures from spherical micelle building blocks.

by which the cylindrical micellar aggregates are thought to be formed. In this scheme, PF rod segments of **tri-PFPVP** tend to parallel packing to protect the insoluble parts by outside coil blocks and gain energy from rod-rod segments stacking along the cylinder axis. When MeOH content is increased continuously, individual long cylinders are forced to aggregate together to reduce interfacial area in the highly poor solvent environment. Together with these topological constraints, the strong $\pi-\pi$ stacking of the PF segments is also believed to contribute significantly to the stabilization of such aggregated structure.

The morphology of cylinder, observed by TEM from **tri-PFPVP** solutions, is also demonstrated by TM-SFM topography in parts A and B of Figure 9 (MEOH/THF w/w = 70/30) for height and phase images, respectively. The average diameter for cylinders from Figure 9(A) or 9(B) is around 35 nm, which is nearly the same value as that obtained from the TEM results. Moreover, Figures 9(C) and (D) illustrate height and phase images for "bundles of cylinder" structure (MEOH/THF ratio = 90/10),[48,49] which is in good agreement with TEM micrographs.

Since SFM and TEM give the structures of the micellar aggregates after evaporation of the solvents, possible artifacts from differential evaporation rates of THF and MeOH cannot be ruled out due to the different vapor pressures of THF and MeOH. Therefore, cryoTEM from vitrified micellar solutions and dynamic light scattering were carried out, to conclusively establish whether the structures presented in Figures 5−9 are the sole result of the selectivity of MeOH for P2VP blocks.

Figure 10 shows the cryoTEM micrographs on vitrified sections from solutions of analogue composition. The left column gives the micellar microstructures observed for the **di-PFPVP** when going through MeOH/THF solvent ratios of (A)

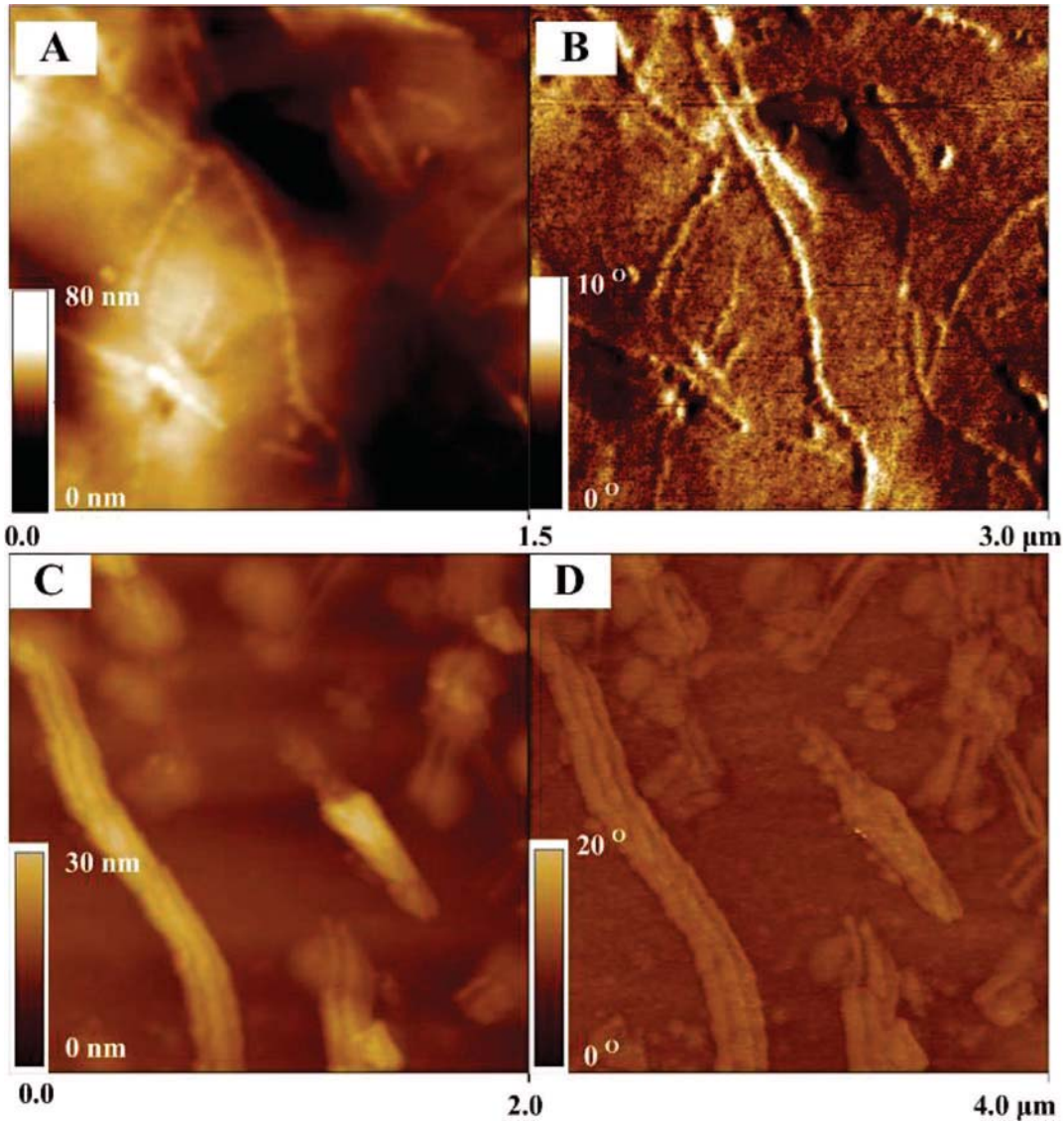

Figure 9. TM-SFM images: on micellar morphologies of **tri-PFPVP** (A) cylinders (height), MeOH/THF = 70/30 (w/w); (B) cylinders (phase), MeOH/THF = 70/30 (w/w); (C) bundle of cylinders (height), MeOH/THF = 90/10 (w/w); (D) bundle of cylinders (phase), MeOH/THF = 90/10 (w/w).

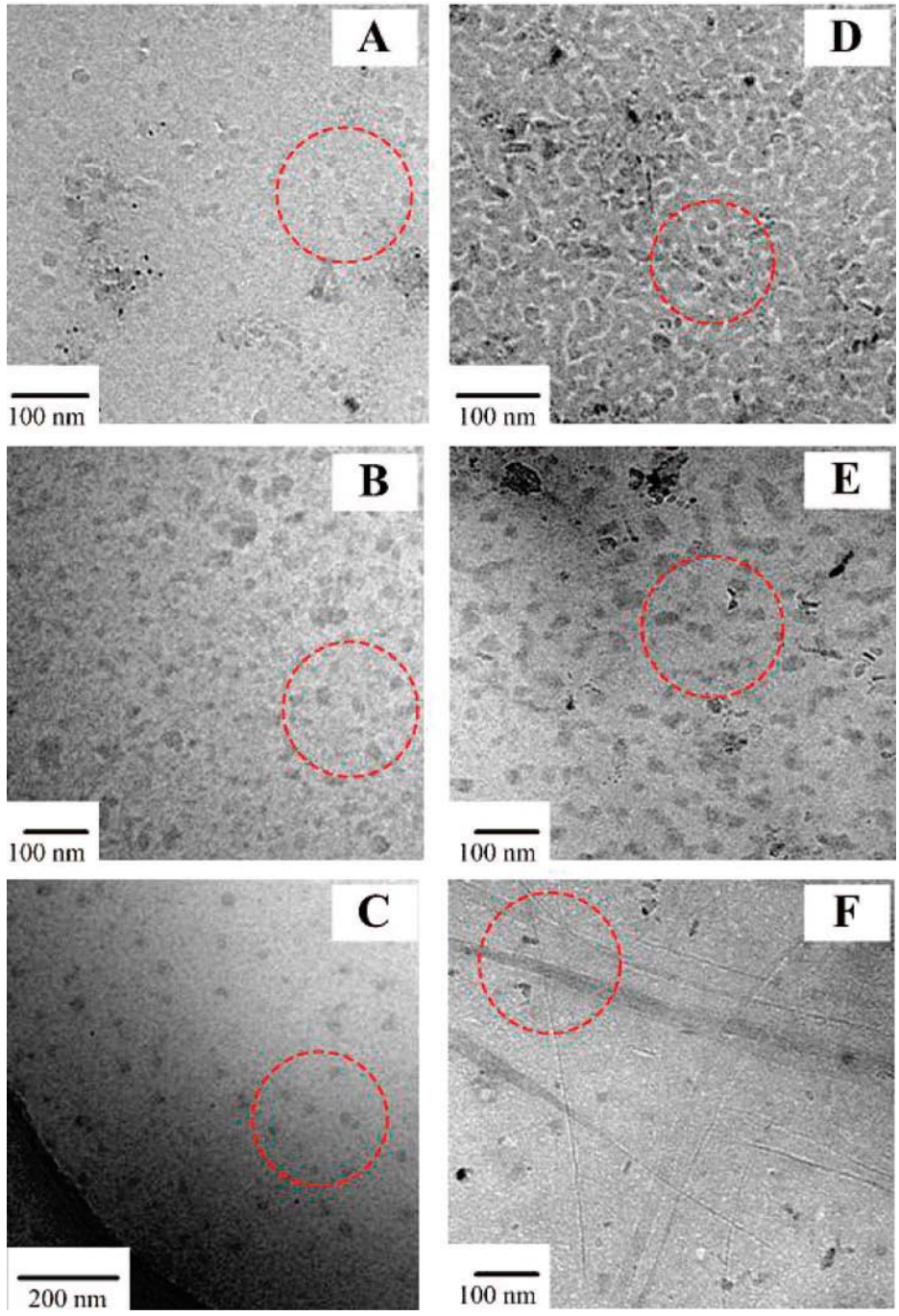

Figure 10. CryoTEM micrographs of **di-PFPVP** and **tri-PFPVP** micellar aggregates in vitrified solutions. **di-PFPVP** micelles in different solvent mixtures with the MeOH/THF weight ratios of (A) 0/100, (B) 30/70, and (C) 60/40, respectively. **tri-PFPVP** micelles in different solvent mixtures with the MeOH/THF weight ratios of (D) 0/100, (E) 30/70, and (F) 60/40, respectively.

0/100, (B) 30/70 and (C) 60/40, while the right column gives the micellar microstructures observed for the **tri-PFPVP** when going through MeOH/THF solvent ratios of (D)0/100, (E)30/70, and (F) 60/40. Indeed, the presence of aggregates already in pure THF are also detectable by cryoTEM, and while in the case of **di-PFPVP** these aggregates are spherical, in the case of **tri-PFPVP** the aggregates are more elongated in shape. Furthermore, also in cryoTEM a great increase in size for the **tri-PFPVP** micelles is also observed with increasingly selective solvent, while the size of **di-PFPVP** micelles is much more unaffected by presence of MeOH. Finally, also the trends of standard TEM and SFM are confirmed, showing that in the case of **di-PFPVP** the micellar aggregates remain spherical while in the case of **tri-PFPVP** a spherical-cylindrical transition occurs upon increasing MeOH. Thus, the aggregate seem to be stable enough to survive the evaporation process without major perturbations.

Hydrodynamic radii were measured by dynamic light scattering (DLS) for both **di-PFPVP** and **tri-PFPVP** in various MeOH/THF compositions, as those used for the cryoTEM experiments. At 100% THF, some aggregates of 30 and 19 nm in size are already present for both **di-PFPVP** and **tri-PFPVP**, respectively. This indicates that THF is a slight selective solvent for the studied block copolymers. By adding 30 wt % of MeOH in the mixed solvent mixture, the solvent has become greatly selective and the aggregate sizes increase, with hydrodynamic radius of 42 and 95 nm for **di-PFPVP** and **tri-PFPVP**, respectively. By a MeOH/THF solvent ratio of 60/40, the measurement on the **tri-PFPVP** becomes impossible due to multiple scattering, indicating the presence of very large objects.

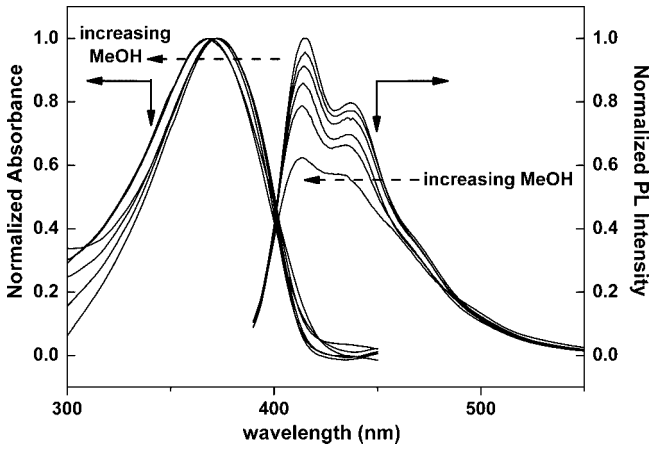

Figure 11. UV−vis absorption and photoluminescence spectra of **di-PFPVP** in different solvent mixtures with the MeOH/THF weight ratios of 0/100, 10/90, 30/70, 50/50, 70/30, and 90/10, respectively.

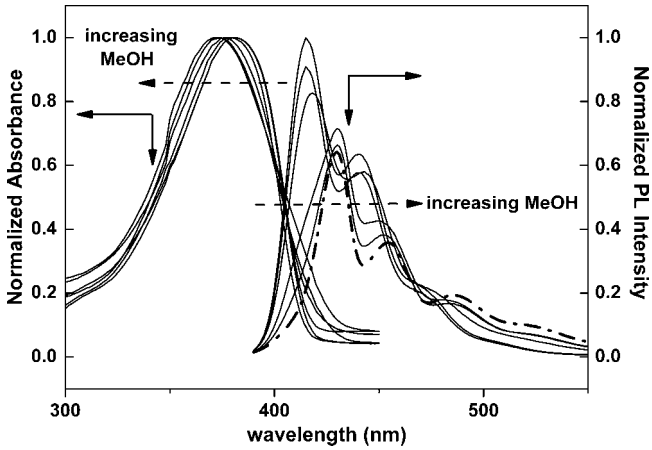

Figure 12. UV−vis absorption and photoluminescence spectra of **tri-PFPVP** in different solvent mixtures with the MeOH/THF weight ratios of 0/100, 10/90, 30/70, 50/50, 70/30, and 90/10, respectively.

However, a hydrodynamic radius of 40 nm can still be obtained for **di-PFPVP** at the same mixture composition, although a slight decrease in the apparent radius suggests that the threshold for multiple scattering is attained at this solvent composition. The micellar morphology from the DLS shows the same trend as those from TEM and TM-SFM.

Photophysical Properties. Photophysical properties were investigated in order to understand the self-assembly of block copolymers in solvent mixtures, reflecting the status of the interchain $\pi-\pi$ stacking of conjugated rod segments.[50−52] Figure 11 shows several results of UV−vis absorption (left) and photoluminescence spectra (right) of **di-PFPVP** in different weight composition of MeOH/THF. The optical absorption peak maximum (λ_{max}) of **di-PFPVP** in THF is observed at 374 nm. As the MeOH content increases, the absorption spectrum has slightly blue-shifting and the λ_{max} shifts to 368 nm at the MeOH/THF weight composition of 90/10. It indicates that the reduction of effective conjugated length in methanol since the PF blocks become less planar to account for aggregate formation with increasing poor solvent content.[36] The corresponding photoluminescence spectra in pure THF show one main peak at 415 nm and one shoulder at 437 nm and the corresponding luminescence quantum efficiency of 0.6 at the excitation wavelength of 370 nm. The addition of MeOH progressively shifts slightly the two emission peaks from 415 to 411 nm and from 437 to 432 nm, respectively. At MeOH/THF solvent ratio of 90/10, the emission quantum efficiency is quenched to 0.40. According to the results of TEM characterization, the worm-like morphology in Figure 5E is presumably arising from a coalescence of spherical micelles. Consequently, the blue-shifted emission peaks from 415 to 411 nm and from 437 to 432 nm accompanied by quenched emission intensity, is observed as a result of adhesion, collision, fusion, and aggregation of spherical micelles at a high MeOH content. The blue shifting and gradually quenching quantum efficiencies of emission spectra suggest a H-type $\pi-\pi$ interchain stacking of the **di-PFPVP** in the MeOH/THF mixed solvent mixture.[53]

Figure 12 shows the UV−vis absorption (left) and photoluminescence spectra (right) of **tri-PFPVP** in different solvent compositions of MeOH/THF. In pure THF, in left side of figure, the absorption peak maximum (λ_{max}) is observed at 380 nm and shows blue-shifting to 374 nm upon increase in MeOH, evidencing the formation of self-assembled structures with increasing selective solvent content. In comparison to **di-PFPVP** in pure THF, the **tri-PFPVP** has a higher λ_{max} at the same PF block length and similar copolymer compositions (380 nm vs 374 nm). It implied that P2VP coil blocks binding in two sides of the PF rod make the copolymer chains having higher symmetric arrangements than the homologue diblock copolymer. Consequently, **tri-PFPVP** polymer chains can stack together favorably and have higher $\pi-\pi$ interchain stacking compared with the **di-PFPVP**, leading to the higher absorption maximum.

The photoluminescence spectrum of **tri-PFPVP** in pure THF shown in Figure 12 has one main peak at 415 nm and two shoulders at 439 and 465 nm. As the MeOH content is increased, the fluorescence intensity decreases and the quantum yield reduces from 0.65 in pure THF to 0.40 in 90/10 ratio of MeOH/THF mixture. Moreover, at the MeOH content of 30 wt %, the peak and shoulders are red-shifted slightly from 415 to 418, 439 to 443 and 465 to 468 nm, respectively. As the MeOH/THF ratio reaches 50/50 or beyond, the expected red-shifting of three emission peaks is observed. The prominent red-shifting on the above peaks and shoulders are observed at 430, 454, and 486 nm (dash-dot line) at MeOH/THF ratio of 90/10, respectively. In addition, the emission intensity of the shoulder located at the highest wavelength (486 nm) becomes more conspicuous than that of the original one, indicating the formation of aggregated excimers. By comparing the photoluminescence results of **tri-PFPVP** with **di-PFPVP,** only the former one shows the expected peak locating at 486 nm for the high MeOH content. This is in agreement with the morphology results indicating that **tri-PFPVP** have higher $\pi-\pi$ interchain stacking compared to **di-PFPVP**, due to symmetric architectures. For the case of the **di-PFPVP**, both UV−vis absorption and photoluminescence spectra show blue-shifting with increasing MeOH, which is consistent with an H-type aggregation. However, for the **tri-PFPVP** blue-shifting for UV−vis absorption is observed together with red-shifting for photoluminescence upon increasing solvent selectivity. This suggests that the effect of polymer architecture on the photophysical properties of conjugated rod−coil copolymers is significant. It is well-known that the J-type aggregation shifts the UV−vis and emission spectra to red, while the H-type aggregation shifts both the UV−vis and emission spectra to blue.[53−55] These findings suggest, however, that the aggregation occurring in **tri-PFPVP** is of another type, which is not consistent with either H-type or J-type. Similar observation on the photophysical properties was also reported in the triblock poly(2-(dimethylamino)ethyl methacrylate)-*block*-polyfluorene-*block*-poly(2-(dimethylamino)-ethyl methacrylate) (PDMAEMA- *b*-PF-*b*-PDMAEMA) system in THF/H_2O.[32]

Conclusions

In this study, new rod−coil block copolymers of PF-*b*-P2VP (**di-PFPVP**) and triblock P2VP-*b*-PF-*b*-P2VP (**tri-PFPVP**) were

successfully synthesized by combining coupling reaction for rod segments and living anionic polymerization for coil segments. The main structural differences of diblock and triblock copolymers were shown to essentially be the morphologies of the micellar aggregates in THF/MeOH mixtures: while the diblock copolymers maintained a spherical micellar aggregates, triblocks were found to readily aggregate in elongated cylinders. The present study suggests the importance of polymer architecture on the aggregated structures for rod−coil and coil−rod−coil block copolymers in dilute solution. We also revealed the effect of polymer chain architecture and the aggregated structures on the photophysical properties. Because **tri-PFPVP** polymer chains can stack together more favorably into cylindrical arrays, they can provide preferential conditions for $\pi-\pi$ interchain stacking compared with the spherical aggregates observed for **di-PFPVP**, leading to the higher absorption maximum. For **di-PFPVP** in presence of MeOH as selective solvent for the P2VP block, H-type aggregates were observed with corresponding blue shifting the UV−vis absorption and photoluminescence spectra upon increasing the concentration of MeOH in the MeOH/THF solvent mixtures. However, **tri-PFPVP** behaves very differently, with the UV−vis absorption shifting to blue and photoluminescence shifting to red upon the same solvent conditions used for the **di-PFPVP**. This behavior indicates a new type of topological aggregates in selective solvents, which is consistent neither with H-type nor J-type aggregation.

Acknowledgment. We express deep thanks for the financial support of the National Science Council (NSC96-2221-E-002-021), Excellent Research Projects of National Taiwan University, and Ministry of Economic Affairs of Taiwan (96-Ec-17-A-08-S1-015). Nicolas Sary (University of Fribourg) and Antti Nykänen (Helsinki University of Technology) are kindly acknowledged for useful discussions.

References and Notes

(1) Chen, D.; Jiang, M. *Acc. Chem. Res.* **2005**, *38*, 494–502.
(2) Alexandridis, P.; Lindman, B. *Amphiphilic Block Copolymers: Self-Assembly and Applications*; Elsevier: Amsterdam, 2000.
(3) Hadjichristidis, N.; Pispas, S.; Floudas, G. A. *Block Copolymers: Synthesis Strategies, Physical Properties, and Applications*; John Wiley & Sons: Hoboken, NJ, 2003.
(4) Mofeitt, M.; Khougaz, K.; Eisenberg, A. *Acc. Chem. Res.* **1996**, *29*, 95–102.
(5) Bates, F. S.; Fredrickson, G. H. *Phys. Today* **1999**, *52*, 32–38.
(6) Fasolka, M. J.; Mayes, A. M. *Annu. Rev. Mater. Res.* **2001**, *31*, 323–355.
(7) Krausch, G.; Magerle, R. *Adv. Mater.* **2002**, *14*, 1579–1583.
(8) Antonietti, M.; Foster, S. *Adv. Mater.* **2003**, *15*, 1323–1333.
(9) Park, C.; Yoon, J.; Thomas, E. L. *Polymer* **2003**, *44*, 6725–6760.
(10) Cheng, J. Y.; Ross, C. A.; Smith, H. I.; Thomas, E. L. *Adv. Mater.* **2006**, *18*, 2505–2521.
(11) Ryu, D. Y.; Lee, D. H.; Jeong, U.; Yun, S. H.; Park, S.; Kwon, K.; Sohn, B. H.; Chang, T.; Kim, J. K.; Russell, T. P. *Macromolecules* **2008**, *37*, 3717–3724.
(12) Lee, D. H.; Han, S. H.; Joo, W.; Kim, J. K.; Huh, J. *Macromolecules* **2008**, *41*, 2577–2583.
(13) Hanley, K. J.; Lodge, T. P.; Huang, C. I. *Macromolecules* **2000**, *33*, 5918–5931.
(14) Li, Z.; Hillmyer, M. A.; Lodge, T. P. *Langmuir* **2006**, *22*, 9409–9417.
(15) Simone, P. M.; Lodge, T. P. *Macromolecules* **2008**, *41*, 1713–1719.
(16) Liu, X. K.; Jiang, M. *Angew. Chem., Int. Ed.* **2006**, *45*, 3846–3850.
(17) Mu, M. F.; Ning, F. L.; Jiang, M.; Chen, D. *Langmuir* **2003**, *19*, 9994–9996.
(18) Dou, H. J.; Jiang, M.; Peng, H. S.; Chen, D. Y.; Hong, Y. *Angew. Chem., Int. Ed.* **2003**, *42*, 1516–1519.
(19) Lee, M.; Cho, B. K.; Zin, W. C. *Chem. Rev.* **2001**, *101*, 3869–3892.
(20) Hoeben, F. J. M.; Jonkhijm, P.; Meijer, E. W.; Schenning, A. P. H. J. *Chem. Rev.* **2005**, *105*, 1491–1546.
(21) Leclère, P.; Hennebicq, E.; Calderone, A.; Brocorens, P.; Grimsdale, A. C.; Mullen, K.; Brédas, J. L.; Lazzaroni, R. *Prog. Polym. Sci.* **2003**, *28*, 55–81.
(22) LecLerc, M. *J. Polym. Sci., Part A: Polym. Chem.* **2001**, *39*, 2867–2873.
(23) Balamurugan, S. S.; Bantchev, G. B.; Yang, Y.; McCarley, R. L. *Angew. Chem., Int. Ed.* **2005**, *44*, 4872–4876.
(24) Olsen, B. D.; Alcazar, D.; Krikorian, V.; Toney, M. F.; Thomas, E. L.; Segalman, R. A. *Macromolecules* **2008**, *41*, 58–66.
(25) Dai, C. A.; Yen, W. C.; Lee, Y. H.; Ho, C. C.; Su, W. F. *J. Am. Chem. Soc.* **2007**, *129*, 11036–11038.
(26) Jenekhe, S. A.; Chen, X. L. *Science* **1998**, *279*, 1903–1907.
(27) Rubatat, L.; Kong, X.; Jenekhe, S. A.; Ruokolainen, J.; Hojeij, M.; Mezzenga, R. *Macromolecules* **2008**, *41*, 1846–1852.
(28) Boudouris, B. W.; Frisbie, C. D.; Hillmyer, M. A. *Macromolecules* **2008**, *41*, 67–75.
(29) Schref, U.; List, E. J. W. *Adv. Mater.* **2002**, *14*, 477–487.
(30) Neher, D. *Macromol. Rapid Commun.* **2001**, *22*, 1365–1385.
(31) Lu, S.; Fan, Q. L.; Liu, S. Y.; Chua, S. J.; Huang, W. *Macromolecules* **2002**, *35*, 9875–9881.
(32) Lu, S.; Fan, Q. L.; Chua, S. J.; Huang, W. *Macromolecules* **2003**, *36*, 304–310.
(33) Lin, S. T.; Y. C., Tung.; Chen, W. C. *J. Mater. Chem.* **2008**, *18*, 3985–3992.
(34) Lu, S.; Liu, T.; Ke, L.; Ma, D. G.; Chua, S. J.; Huang, W. *Macromolecules* **2005**, *38*, 8494–8502.
(35) Chochos, C. L.; Tsolakis, P. K.; Gregoriou, V. G.; Kallitis, J. K. *Macromolecules* **2004**, *37*, 2502–2510.
(36) Tung, Y. C.; Wu, W. C.; Chen, W. C. *Macromol. Rapid Commun.* **2006**, *27*, 1838–1844.
(37) Marsitzky, D.; Klapper, M.; Mullen, K. *Macromolecules* **1999**, *32*, 8685–8688.
(38) Hirao, A.; Hayashi, M.; Loykulnant, S.; Sugiyama, K.; Ryu, S. W.; Haraguchi, N.; Matsuo, A.; Higashihara, T. *Prog. Polym. Sci.* **2005**, *30* (2), 111–182.
(39) Hirao, A.; Loykulnant, S.; Ishizone, T. *Prog. Polym. Sci.* **2002**, *27*, 1399–1471.
(40) Rahman, M. S.; Samal, S.; Lee, J. S. *Macromolecules* **2007**, *40*, 9279–9283.
(41) Sary, N.; Rubatat, L.; Brochon, C.; Hadziioannou, G.; Ruokolainen, J.; Mezzenga, R. *Macromolecules* **2007**, *40*, 6990–6997.
(42) Klarner, G.; Lee, J. I.; Lee, V. Y.; Chan, E.; Chen, J. P.; Nelson, A.; Markiewicz, D.; Siemens, R.; Scott, J. C.; Miller, R. D. *Chem. Mater.* **1999**, *11*, 1800–1805.
(43) Zhang, L.; Eisenberg, A. *Polym. Adv. Technol.* **1998**, *9*, 677–699.
(44) Burke, S. E.; Eisenberg, A. *Langmuir* **2001**, *17*, 8341–8347.
(45) Zhang, L. F.; Eisenberg, A. *Science* **1995**, *268*, 1728–1731.
(46) Zhu, J.; Yu, H.; Jiang, W. *Macromolecules* **2005**, *38*, 7492–7501.
(47) Du, H.; Zhu, J.; Jiang, W. *J. Phys. Chem. B* **2007**, *111*, 1938–1945.
(48) Cheng, C. X.; Huang, Y.; Tang, R. P.; Chen, E.; Xi, F. *Macromolecules* **2005**, *38*, 3044–3047.
(49) Ryu, J. H.; Lee, M. *J. Am. Chem. Soc.* **2005**, *127*, 14170–14171.
(50) Li, K.; Wang, Q. *Macromolecules* **2004**, *37*, 1172–1174.
(51) Wu, W. C.; Tian, Y.; Chen, C.-Y.; Lee, C. S.; Sheng, Y.-J.; Chen, W. C.; A., K.-Y. Jen *Langmuir* **2007**, *23*, 2805–2814.
(52) Sary, N.; Mezzenga, R.; Brochon, C.; Hadziioannou, G.; Ruokolainen, J. *Macromolecules* **2007**, *40*, 3277–3286.
(53) Huo, H.; Li, K.; Wang, Q.; Wu, C. *Macromolecules* **2007**, *40*, 6692–6698.
(54) de Cuendias, A.; Le Hellaye, M.; Lecommandoux, S.; Cloutei, E.; Cramail, H. *J. Mater. Chem.* **2005**, *15*, 3264–3267.
(55) Mori, T.; Watanabe, T.; Minagawa, K.; Tanaka, M. *J. Polym. Sci., Part A: Polym. Chem.* **2005**, *43*, 1569–1578.